



Effect of dead layer and strain on the diffuse phase transition of PLZT relaxor thin films

S. Tong^{a,b,*}, M. Narayanan^a, B. Ma^a, R.E. Koritala^c, S. Liu^a, U. (Balu) Balachandran^a, D. Shi^b

^a Energy Systems Division, Argonne National Laboratory, Argonne, IL 60439, USA

^b School of Energy, Environmental, Biological and Medical Engineering, University of Cincinnati, Cincinnati, OH 45221, USA

^c Material Science Division, Argonne National Laboratory, Argonne, IL 60439, USA

Received 28 May 2010; received in revised form 27 October 2010; accepted 31 October 2010

Abstract

Bulk relaxor ferroelectrics exhibit excellent permittivity compared to their thin film counterpart, although both show diffuse phase transition (DPT) behavior unlike normal ferroelectrics. To better understand the effect of dead layer and strain on the observed anomaly in the dielectric properties, we have developed relaxor PLZT (lead lanthanum zirconate titanate) thin films with different thicknesses and measured their dielectric properties as a function of temperature and frequency. The effect of dead layer on thin film permittivity has been found to be independent of temperature and frequency, and is governed by the Schottky barrier between the platinum electrode and PLZT. The total strain (thermal and intrinsic) in the film majorly determines the broadening, dielectric peak and temperature shift in the relaxor ferroelectric. The Curie–Weiss type law for relaxors has been further modified to incorporate these two effects to accurately predict the DPT behavior of thin film and bulk relaxor ferroelectrics. The dielectric behavior of thin film is predicted by using the bulk dielectric data from literature in the proposed equation, which agree well with the measured dielectric behavior.

© 2010 Acta Materialia Inc. Published by Elsevier Ltd. All rights reserved.

Keywords: PLZT; Ferroelectric relaxor thin film; Diffuse phase transition; Dead layer; Intrinsic strain

1. Introduction

Since the discovery of lead lanthanum zirconate titanate $\text{Pb}_{1-x}\text{La}_x(\text{Zr}_y\text{Ti}_{1-y})\text{O}_3$ (PLZT) in 1971 [1–3], relaxor ferroelectric compositions have been widely investigated in both bulk and thin films. The unique feature of this class of compounds is their diffuse phase transition (DPT), i.e. lacking of sharp permittivity peak with temperature [4,5]. Among all the perovskite relaxor ferroelectrics, PLZT is the most widely studied mixed A-site perovskite system due to dispersion being enhanced by increasing the lanthanum doping level, a key to understanding this behavior from the

standpoint of lattice structures. It is widely believed that the characteristic DPT behavior in bulk relaxors stems from the complex structure, with more than one type of ion occupying equivalent lattice sites and the large difference in their valence and radii (e.g. PLZT whose A-site includes both lead and lanthanum ions) [4,6–8]. These cationic species induce polar regions in the nanometer scale with dipole moments distributed in random directions between the Burns temperature (T_B) and freezing temperature (T_f), making relaxors behave more like a glass than a crystal [4,7,9]. These polar clusters dramatically affect the nature of the crystal, giving rise to unique physical properties.

Models explaining DPT behavior in bulk relaxors are well developed; however, they fail at the nanometer scale. This is due to the effect of other factors, such as dead layer and strain, that cannot be ignored at these dimensional levels [10–13]. Much progress has been made to explain this

* Corresponding author at: Energy Systems Division, Argonne National Laboratory, Argonne, IL 60439, USA. Tel.: +1 630 252 6516; fax: +1 630 252 3604.

E-mail address: stong@anl.gov (S. Tong).

phenomenon (bulk to thin film) on normal ferroelectric ceramics. It is now widely accepted that the phase transition order changes from first to second as the dimension decreases from bulk to thin film. This is due to the so-called “clamping effects” from the substrates upon which the films are deposited [14]. It is confirmed by the observation of bulk-like phase transition in free-standing (stress-free) ferroelectric thin films [11,15]. However, a similar study has not been carried out on relaxor ferroelectrics, in which the order of phase transition does not change from bulk to thin film. In this paper, we studied the effect of dead layer and strain on the DPT behavior in relaxor-based PLZT (8/52/48) by depositing thin films of varying thicknesses. The experimental data were fitted with the Curie–Weiss law. A modified equation was developed to predict the behavior of relaxor thin films.

2. Experimental procedure

$\text{Pb}_{1-x}\text{La}_x(\text{Zr}_y\text{Ti}_{1-y})\text{O}_3$ (8/52/48) stock solutions were prepared by “inverted mixing order” sol–gel route based on acetic acid chemistry [16]. The starting precursors were 99% lead acetate tri-hydrate, 97% titanium isopropoxide, 70% zirconium *n*-propoxide in 1-propanol and 99.9% lanthanum acetate hydrate (all from Sigma–Aldrich Co.). In brief, zirconium *n*-propoxide and titanium isopropoxide were first mixed and chelated with acetic acid. Lead acetate and lanthanum acetate were mixed in sequence in acetic acid and dissolved by heating to 105 °C. Appropriate amounts of *n*-propanol and de-ionized water were added to obtain a volume ratio of acetic acid, *n*-propanol and water of 15:15:2 to achieve a final concentration of 0.5 M. The solution contains 20 mol.% excess lead to compensate for the lead loss during crystallization heat treatments. The solution was aged for 24 h before thin film

deposition. PLZT thin films with different thicknesses were deposited on platinum coated silicon substrates (Nova Electronic Materials, Inc.).

PLZT layers were prepared by spin-coating the stock solution through 0.02 μm filter (Whatman International Ltd.) onto platinum coated silicon (Pt–Si) at 3000 rpm for 30 s. Each layer was pyrolyzed at 325 °C for 10 min and crystallized at 650 °C for 5 min. The films were crystallized for an extra 5 min every three layers. This process was repeated to achieve films of desired thickness and the films were exposed to a final crystallization anneal of 650 °C for 15 min to ensure uniform perovskite phase. Films containing 3, 5, 10 and 19 layers were fabricated. Platinum top electrodes (250 μm diameter and 100 nm thick) were deposited through a shadow mask by electron-beam evaporation. Dielectric measurements were made as a function of temperature (50–300 °C) and frequency (1–100 kHz) with an Agilent E4980A LCR meter using an oscillator level of 0.1 V in conjunction with a Signatone QuieTemp[®] probe station with hot stage (Lucas Signatone Corp., Gilroy, CA). DC leakage current measurements were made using a Keithley 237 high-voltage source meter. Phase identification was carried out using a Bruker AXS diffractometer with General Area Detector Diffraction System while microstructure and thickness were characterized using a SEM Hitachi S4700 field-emission scanning electron microscope.

3. Results and discussion

3.1. PLZT Thin film characterization

Scanning electron microscopy (SEM) image of the surface of a five layer PLZT film is shown in Fig. 1a. As can be seen in this figure, the microstructure is dense and uniform as expected of films deposited on Pt–Si. The average

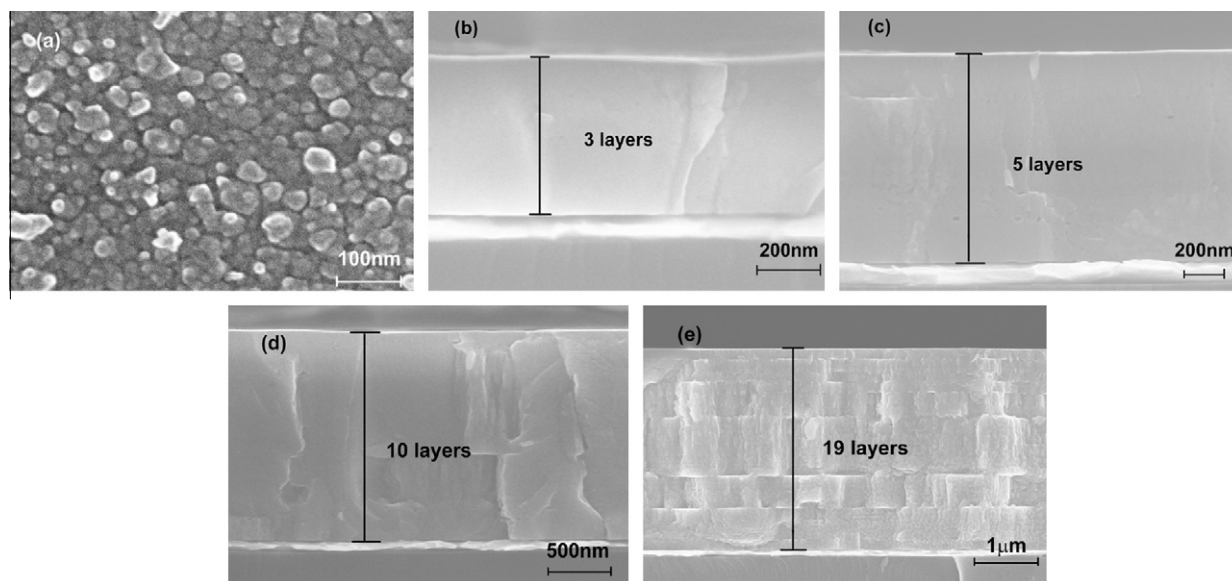


Fig. 1. Scanning electron microscope images of (a) surface and (b–e) cross-sections of PLZT film on Pt–Si substrate. Illustrated in (b–e) are the cross-sectional images of 3-, 5-, 10-, and 19-layer PLZT film, respectively, with corresponding thicknesses of 0.495 μm , 0.825 μm , 1.65 μm , and 3.135 μm .

grain size of the unimodal distribution estimated using ASTM Standard E112-88 is ~ 39.5 nm, which is comparable to the typical PZT/PLZT films obtained using acetic acid sol–gel chemistry [17–19]. The cross-sectional SEM images of 3-, 5-, 10- and 19-layer PLZT thin film on silicon substrate are illustrated in Fig. 1b–e, respectively. All films display a dense, columnar microstructure that is nucleated at the bottom electrode. These films do not contain any obvious defects or other secondary phases (confirmed by XRD in Fig. 2a). The corresponding thickness measured for a 3-, 5-, 10- and 19-layer film are 0.495 μm , 0.825 μm , 1.650 μm , and 3.135 μm , respectively. This corresponds to a constant value of 0.165 μm per layer using the deposition conditions.

The crystal structure and lattice parameter of the PLZT films were determined using the XRD operated in the θ – 2θ scan mode. Fig. 2a shows the out-of-plane diffraction patterns of PLZT thin films with different thicknesses. It is observed that all the films are well crystallized without

the presence of any secondary pyrochlore phase. The intensity of the major tetragonal (1 1 0) reflection increases dramatically with increasing film thickness. The FWHM for the (1 1 0) peak varies between 0.288 and 0.326 for films with different thickness, indicating that these films are well crystallized with fine and similar grain size. Although the grain sizes are small, for columnar structures like that observed in PLZT the effect of grain size on the dielectric behavior is usually dominant only in films where the thickness is similar to the grain size, i.e. aspect ratio (film thickness/grain size) is ≤ 1 . When the aspect ratio is > 3 – 4 the measured dielectric properties are determined by the larger dimension of the grain, which is the length of the columnar grain or the thickness of the film. This is related to the response of the dielectric grain to the direction of the field applied [11,16,20]. Therefore, the effect of surface grain size on the permittivity is ignored in this analysis.

The out-of-plane lattice parameters calculated for tetragonal PLZT from the diffraction patterns obtained for films with different thicknesses are shown in the inset on the right side of Fig. 2a. It can be noted that the lattice parameters vary within $\pm 0.14\%$ for films with different thickness and it falls within the measurement error of the XRD instrument. The lattice parameters (a , 4.009 Å; c , 4.018 Å) are lower than that reported in the literature for bulk PLZT (8/53/47) [2,21], which is due to the tensile stress in the film caused by the difference in the thermal expansion coefficients between the substrate and the dielectric. The in-plane total strain (x_{total}) can be calculated using the following equation:

$$x_{\text{total}} = \frac{a_{\text{out-of-plane}} - a_0}{a_0} \cdot \left(-\frac{2\nu_f}{1 - \nu_f} \right) \quad (1)$$

where $a_{\text{out-of-plane}}$ is out-of-plane lattice parameter calculated from θ – 2θ scan XRD and a_0 is strain-free lattice parameter ($= 4.051$ Å [2,21]). The Poisson's ratio (ν_f) is taken as 0.29 for PLZT after Ref. [22]. The calculated total strain in the film for different thickness is $0.80 \pm 0.08\%$ as illustrated in the inset on the right of Fig. 2a. There is no appreciable variation in the strain with thickness and this observation can be expected as the ratio of the substrate to film thickness is > 160 .

The origin of strain in the polycrystalline film is from: (1) within the film – grain boundary, domain walls and capillary pressure; and (2) between substrate and film – misfit strain and thermal strain [23]. However, the strains are categorized into two groups for convenience in this work: (a) intrinsic strain ($x_{\text{intrinsic}}$), representing the temperature-independent strain; and (b) thermal strain (x_{thermal}), representing the temperature-dependent strain. x_{thermal} can be calculated as follows:

$$x_{\text{thermal}} = \int_T^{T_d} (\alpha_f - \alpha_s) dT \approx \Delta\alpha \cdot (T_d - T) \quad (2)$$

where α_f and α_s are the thermal expansion coefficients of PLZT and Si substrate, respectively, T_d is the crystallization temperature, and T is the temperature at which the

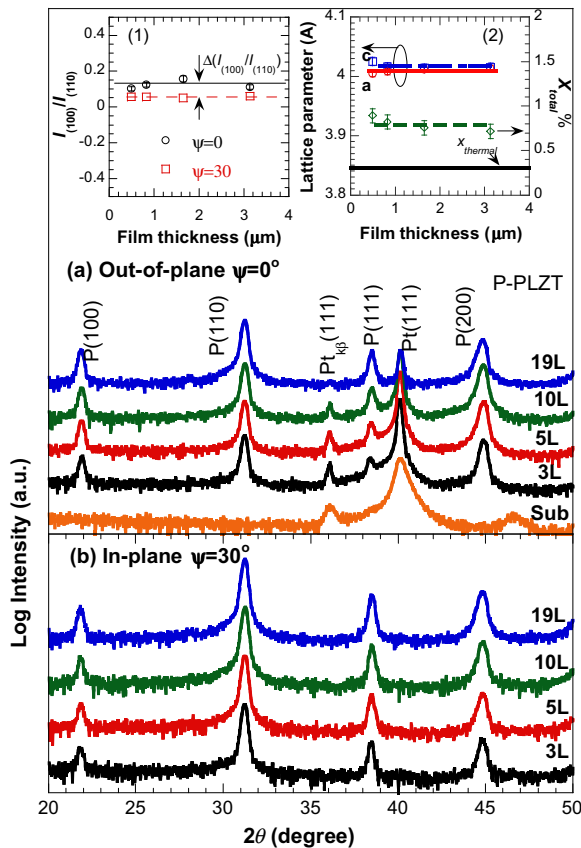


Fig. 2. X-ray diffraction patterns of 3-, 5-, 10-, and 19-layer PLZT film on Pt-Si substrate: (a) out-of-plane XRD patterns with $\psi = 0^\circ$ and (b) in-plane XRD pattern with $\psi = 30^\circ$. The inset on the left shows the intensity ratio between (1 0 0) and (1 1 0) planes for films with different thicknesses in (a) and (b). A constant $\Delta(I_{(100)}/I_{(110)}) = (6.8 \pm 1.8)\%$ between out-of-plane and in-plane XRD indicates a constant intrinsic strain existing in the partial oriented PLZT thin films in the four samples. The inset on the right shows the variation in the lattice parameters (a , c), total strain (x_{total}) calculated from the diffraction patterns as a function of PLZT film thickness, and the thermal expansion (x_{thermal}). Data include error bars calculated from (1 0 0), (1 1 0) and (1 1 1) faces calculated using MDI Jade 5.0.

strain is calculated. The calculated thermal strain is 0.15% using $\alpha_f = 5.4 \times 10^{-6} \text{ }^\circ\text{C}^{-1}$ [3,22], $\alpha_s = 3 \times 10^{-6} \text{ }^\circ\text{C}^{-1}$ [22], $\Delta\alpha = \alpha_f - \alpha_s = 2.4 \times 10^{-6} \text{ }^\circ\text{C}^{-1}$ and $(T_d - T) = 625 \text{ }^\circ\text{C}$. Therefore, the intrinsic strain can be obtained using the following equation:

$$x_{\text{total}} = x_{\text{intrinsic}} + x_{\text{thermal}} = x_{\text{intrinsic}} + \Delta\alpha \cdot (T_d - T) \quad (3)$$

$x_{\text{intrinsic}}$ calculated using Eqs. (1)–(3) is 0.65% at the deposition temperature T_d [24,25]. The intensity ratios of face (100) to (110) with grazing angle $\psi = 30^\circ$ in Fig. 2b are smaller than the ones in Fig. 2a with $\psi = 0^\circ$. The detailed results in Fig. 2a inset on the left indicate invariable intensity ratio among four films at the grazing angle but a constant of 6.8% as a result of 30° difference of grazing angle. It confirms an even intrinsic strain existing in all films.

3.2. PLZT thin film phase transition

To investigate the evolution and nature of DPT behavior in PLZT relaxor thin films, we measured the relative permittivity and dielectric loss ($\tan \delta$) of films with different thicknesses at various temperatures in the range 50–300 $^\circ\text{C}$, as illustrated in Fig. 3a. The “relative permittivity” is also referred as “permittivity” throughout the text below for convenience. In general, it can be observed that the permittivity increases dramatically from 1200 to 2100 for film thicknesses below 1.6 μm and does not vary significantly beyond that thickness. Peaks in the permittivity response as a function of temperature are typically expected in dielectric materials, signifying the different phase transitions that occur in the material. The maximum permittivity (ϵ_m) corresponding to a temperature (T_m) signifying the onset of tetragonal to cubic phase transition in relaxor

PLZT (8/52/48), was not observed for the three-layer film. At the same time the diffuse nature of the phase transition can be clearly noticed in 5-, 10-, and 19-layer films (Fig. 3a), with T_m at $\sim 150 \text{ }^\circ\text{C}$. On the other hand, the dielectric loss response was relatively flat for all the samples in the temperature range measured. Unlike the permittivity response the dissipation factor does not follow a certain trend with film thickness, as it is viewed as an extrinsic property dominated by the number and type of physical defects in the films rather than the intrinsic property of the material [26]. Since these films were fabricated simultaneously using the same stock solution under identical processing conditions, these films can be expected to have similar degree of chemical heterogeneity and its effect on temperature-dependent dielectric properties can be ignored in this comparative study. This is further confirmed by the fact that the maximum permittivity temperature is thickness-independent, as observed in Fig. 3a.

It should be pointed out that the maximum permittivity temperature, T_m , is different from the Curie temperature (T_c), due different dipole dynamics in the polar nano-regions (PNR) associated with the dispersive nature in the temperature dependence of the permittivity at all frequencies [4,7,9]. In relaxors, the Curie–Weiss law (linear relation between inverse permittivity and temperature) holds well only for temperatures above T_B , and for temperatures between T_m and T_B , it follows the power law as shown in the following equation:

$$\frac{1}{\epsilon_r} - \frac{1}{\epsilon_m} = \frac{(T - T_m)^n}{2\epsilon_m \delta_m^2} \quad (4)$$

where ϵ_m is the dielectric constant at T_m , δ_m is the shape parameter and $n = 1$ –2 indicating the extent of dispersion or diffuse phase transition. When $n = 1$, Eq. (4) becomes

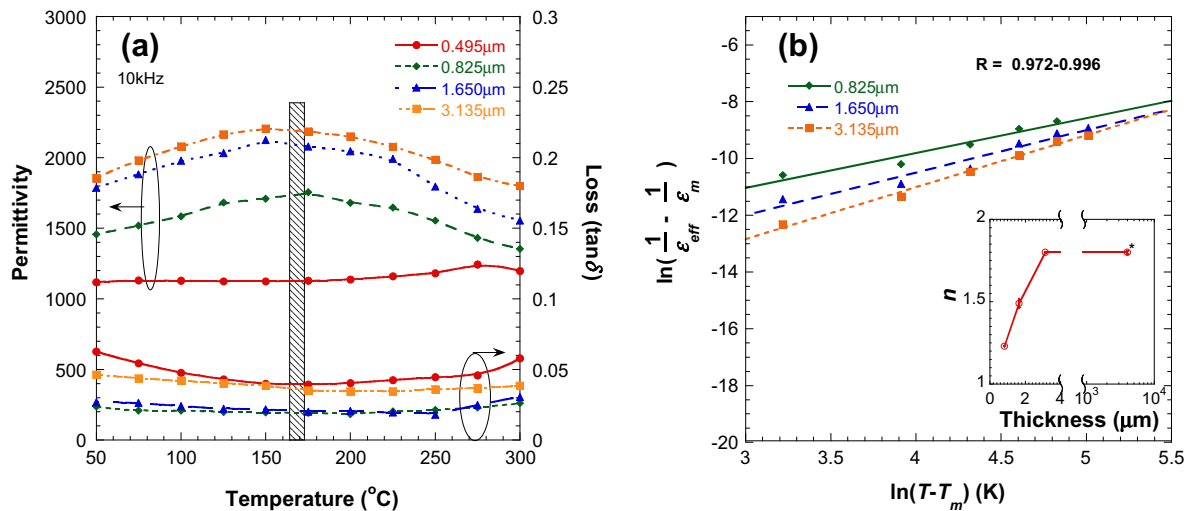


Fig. 3. (a) Permittivity and loss measured as a function of temperature for PLZT films of various thicknesses. Shaded area represents the range of T_m reported for bulk PLZT (8/53/47). Ref. [21] measured at different frequency. (b) Illustrates the diffuse phase transition function fit using Eq. (4) for 5-, 10-, and 19-layer PLZT film. The inset shows the dispersion factor n as a function of film thickness calculated from the slope of the fitting. The fitting parameter (R) obtained ranges between 0.972 and 0.996. The dispersion factor calculated for bulk PLZT (8/53/47) from Ref. [21] (represented as a star) is also shown for comparison.

the Curie–Weiss law used for the normal ferroelectric phase transition; and when $n = 2$ it describes the totally diffuse phase transition nature in bulk relaxors.

Fig. 3b is obtained by using Eq. (4) to the measured data in Fig. 3a to calculate the dispersion factor n . The slope of the fitted lines corresponds to the dispersion factor for films with different thicknesses and is shown in the inset of Fig. 3b. The dispersion factor cannot be calculated for the three-layer film due to absence of an obvious T_m . It was noticed that the dispersion factor increases rapidly with film thickness and achieves a value of 1.8. This may be attributed to: (1) decrease in the intrinsic strain and substrate clamping effects [27,28]; and (2) decrease in the effect of dead layer to the effective permittivity [10,15,29]. These factors have been extensively discussed in the literature and have been the real hindrance to the development of thin film capacitor (rather than bulk) for different applications [4,9,30]. The dispersion factor for a bulk PLZT ceramic reported in the literature [21] was calculated using Eq. (4) and is represented as a “star” in the inset for comparison. It can be concluded that the dispersion factor is ~ 1.8 for films $> 3 \mu\text{m}$ in thickness, close to values observed in bulk [21].

3.3. Dead layer effect to the diffuse phase transition of PLZT thin films

The dead layer is believed to exist between the electrode or substrate and dielectric layers and has a low permittivity compared to the dielectric (this is not to be confused with interfacial layer caused by inter-diffusion of chemical species or formation of secondary phase). This dead layer is an intrinsic effect caused by the metal–dielectric contact induced potentials or depolarizing field rather than defects or strain field [15,29]. This leads to a low effective series capacitance (permittivity) measured in the resultant thin film capacitors. To estimate the contribution of the dead layer to the dielectric dispersion, the equivalent series capacitor model was used, namely Eqs. (5) and (6):

$$\frac{1}{C_{\text{eff}}} = \frac{1}{C_{\text{thin}}} + \frac{1}{C_{\text{dead}}} \quad (5)$$

$$\frac{t}{\epsilon_{\text{eff}}} = \frac{t}{\epsilon_{\text{thin}}} + t_{\text{dead}} \left(\frac{1}{\epsilon_{\text{dead}}} - \frac{1}{\epsilon_{\text{thin}}} \right) \approx \frac{t}{\epsilon_{\text{thin}}} + \frac{t_{\text{dead}}}{\epsilon_{\text{dead}}} \quad (6)$$

where C , ϵ , and t are the capacitance, relative permittivity and thickness, respectively, while subscripts “thin” and “dead” represent dielectric thin film and dead layer. The subscript “eff” represents the effective response being directly measured using the LCR meter. The total thickness (t) is the film thickness measured using SEM (Fig. 1). In Eq. (6), the term $t_{\text{dead}}/\epsilon_{\text{thin}}$ is neglected because $\epsilon_{\text{thin}} \gg \epsilon_{\text{dead}}$.

Using Eq. (6) with the measured data in Fig. 3, the thickness over permittivity is plotted as a function of thickness at different temperatures in Fig. 4. Measurements were made at intervals of 25°C in the temperature range 50 – 300°C and at various frequencies (1, 10, 50 and

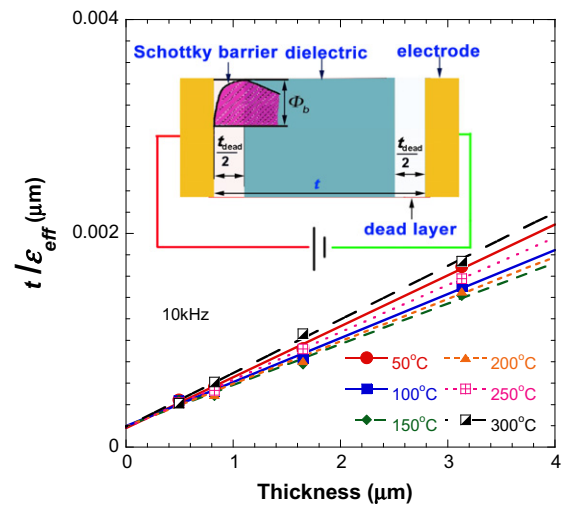


Fig. 4. Plot of inverse permittivity (t/ϵ_{eff}) as a function of PLZT thickness measured at different temperatures. Measurements were made at intervals of 25°C in the temperature range and only six are shown for clarity. Measurements were also carried out at 1, 50 and 100 kHz while only the results from 10 kHz tests are shown ($0.9966 < R < 0.9996$). Inset illustrates the presence of the dead layer effect caused by the Schottky barrier that exists between the metal electrode and the dielectric insulator.

100 kHz), but only six temperatures are shown in Fig. 4 for clarity. The data are fitted with a linear line; the intercept at “zero” thickness would give the contribution from the dead layer and the slope represents the inverse thin film permittivity. It is noticed from Fig. 4 that the intercepts ($t_{\text{dead}}/\epsilon_{\text{dead}}$) for various lines are independent of temperature and frequency while permittivity without dead layer effect varies according to temperature and frequency (detailed data are shown in Fig. 5). The fitting parameter R ranges between 0.9966 and 0.9996, indicating an excellent fit using Eq. (6). The frequency- and temperature-independent intercept was found to be 0.2 nm. Since the dead

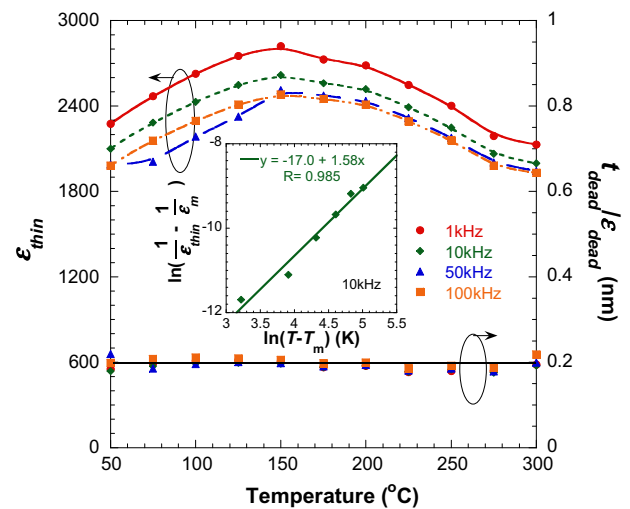


Fig. 5. Calculated thin film permittivity compensated with dead layer effect and dead layer parameter ($t_{\text{dead}}/\epsilon_{\text{dead}}$) as a function of temperature for PLZT films at various frequencies. Inset shows the fitting of Eq. (6) for thin film permittivity compensated with dead layer effect at 10 kHz. The slope of this fit gives the dispersion parameter n .

layer contribution is independent of temperature and frequency, it is likely related to the electronic screening between the electrode and the dielectric. We therefore measured the DC leakage current with increasing field as a function of temperature for films with different thickness, as shown in Fig. 6 [31,32].

It can be observed in Fig. 6 that the leakage current density, $\ln(J)$, follows a linear relationship between the applied field ($E^{0.5}$) for all thicknesses and temperature. This behavior can be described by the Schottky and modified space-charge limited current model according to Ref. [32] as follows:

$$J = A^{**} T^2 \exp \left[-\frac{1}{kT} \left(q\Phi_b - q \sqrt{\frac{qE_0}{4\pi\epsilon_0(\epsilon_r)_{\text{barrier}}}} \right) \right] \quad (7)$$

where J is the current density, A^{**} the Richardson constant, T the temperature, Φ_b the Schottky barrier height, q the elementary charge, k the Boltzmann constant, E_0 the electric field at the metal/insulator interface, ϵ_0 the permittivity of free space, and $(\epsilon_r)_{\text{barrier}}$ the equivalent Schottky relative permittivity. The data are fit with Eq. (7), and $(\epsilon_r)_{\text{barrier}}$ is calculated to be 4.2 ± 1.1 , which is again temperature- and thickness-independent. This value may be considered as the permittivity of the dead layer (ϵ_{dead}) and the thickness of the dead layer (t_{dead}) is calculated to be 0.84 nm, which corresponds to 0.42 nm on each side of the dielectric [33]. These results partially explain that the dead layer effect is primarily based on the Schottky barrier between the electrode and dielectric layer rather than other factors [29,34–36].

By compensating the contribution of the dead layer ($t_{\text{dead}}/\epsilon_{\text{dead}}$) to the equivalent series capacitance model of Eq. (6), the true permittivity of the thin film, ϵ_{thin} , is calculated and presented in Fig. 5. The permittivity shows bulk-like diffuse phase transition which is frequency-dependent. The permittivity reaches its peak at 150 °C for all frequency

and it is the same when the dead layer effect is not compensated (Fig. 3a). This indicates that the dead layer affects only the magnitude of the permittivity without drifting in T_m . The inset of Fig. 5 shows that the dispersion factor n is equal to 1.6 and is lower than 1.8 observed in the case of bulk, where the effect of dead layer can be ignored. Although the dead-layer-compensated thin film permittivity is higher than that in Fig. 3a, it is significantly lower than that reported in bulk PLZT ceramics [21]. These suggest that other factors contribute to this anomaly seen in thin films. Since these perovskite materials are ferroelastic in nature and thin films grown on substrates are under tremendous stress (due to thermal and intrinsic), effect of strain cannot be ignored in understanding the dielectric behavior. Ong et al. [37] studied the effect of strain on the permittivity of ferroelectric films and found that the permittivity was determined by the residual stress and the thickness of the films. We thus attempted to compensate for strain into the model as discussed below.

3.4. Strain effect on diffuse phase transition of the PLZT thin films

Stress in the plane causes a change in the permittivity measured through the thickness according to the following relation [24,28]:

$$\frac{1}{\epsilon_{\text{thin}}} = \frac{1}{\epsilon_{\text{bulk}}} - 4\epsilon_0 Q_{12} \frac{E_f}{1 - \nu_f} x_{\text{total}} \quad (8)$$

where E_f , ν_f , Q_{12} are the Young's modulus, Poisson's ratio and electrostrictive coefficient of the bulk composition, respectively [24,28]. Values used in the calculation are $E_f = 85$ GPa, $\nu_f = 0.29$ [22], $Q_{12} = -0.01$ m⁴ C⁻² [3]. It is assumed that the $x_{\text{intrinsic}}$ is primarily defined by the intrinsic strain between the dielectric layer and substrate at the crystalline temperature (T_d) and is insensitive to temperature,

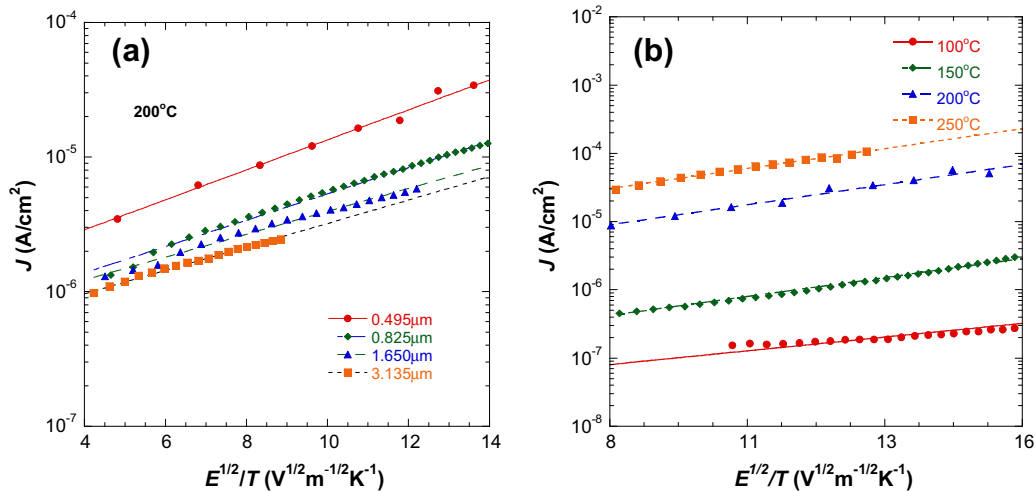


Fig. 6. Measured leakage current density is plotted against increasing electric field of: (a) PLZT film with different thicknesses at 200 °C, and (b) three-layer (0.495 μm) thick PLZT film at different temperatures. The lines are the fits obtained using Eq. (7) with R ranging between 0.983 and 0.998. This fit is used to calculate $(\epsilon_r)_{\text{barrier}}$.

i.e. there is no stress relaxation in the temperature range measured.

Bokov et al. [38] modified the empirical formula given in Eq. (4) by using $n = 2$ and fitting to an arbitrary peak temperature T_A to describe frequency-independent high temperature slope of permittivity peak. This method has its advantage in evaluating the extent of dispersion because only one shape parameter δ_A is sufficient to describe the permittivity in a wide temperature range above T_m , as illustrated in the following equation:

$$\frac{1}{\epsilon_r} - \frac{1}{\epsilon_A} = \frac{(T - T_A)^2}{2\epsilon_A \delta_A^2} \quad (9)$$

Eq. (9) is true for both bulk and thin film relaxors. By simply substituting Eqs. (3) and (8) into Eq. (9), we get the following equation:

$$\frac{1}{\epsilon_{thin}} = \left\{ \frac{1}{(\epsilon_A)_{bulk}} + \frac{[T - (T_A)_{bulk}]^2}{2(\epsilon_A)_{bulk}(\delta_A)_{bulk}^2} \right\} - 4\epsilon_0 Q_{12} \frac{E_f}{1 - \nu_f} [x_{intrinsic} + \Delta\alpha(T_d - T)] \quad (10)$$

By comparing Eq. (10) to Eq. (9) and equating the terms we derive the following (Eqs. (11)–(13)):

$$\begin{aligned} \Delta T_A &= (T_A)_{bulk} - (T_A)_{thin} \\ &= -4\epsilon_0 Q_{12} \frac{E_f}{1 - \nu_f} \Delta\alpha(\epsilon_A)_{bulk}(\delta_A)_{bulk}^2 \end{aligned} \quad (11)$$

$$\frac{1}{(\epsilon_A)_{thin}} = \frac{1}{(\epsilon_A)_{bulk}} - 4\epsilon_0 Q_{12} \frac{E_f}{1 - \nu_f} \times \left\{ x_{intrinsic} + \Delta\alpha \left[T_d - (T_A)_{bulk} + \frac{\Delta T_A}{2} \right] \right\} \quad (12)$$

$$(\epsilon_A)_{bulk}(\delta_A)_{bulk}^2 = (\epsilon_A)_{thin}(\delta_A)_{thin}^2 \quad (13)$$

It can be concluded from Eq. (11) that the difference in the arbitrary temperature between the bulk and thin film is determined only by the thermal (α), mechanical (E , ν) and electrical (Q) properties of the bulk relaxor rather than the strain/stress level. However, this is not entirely true because the nano-domains start to grow when the temperature drops below T_B and $\Delta\alpha$ is a function of temperature. In our case this difference in the arbitrary temperature is small or negligible [1,3,9]. Another limitation is that the $x_{intrinsic}$ can be decreased with temperature due to partial cancellation of the strain by the formation of dislocation and poly-domains [14]. In other words Q_{12} and $E_f/(1 - \nu_f)$ are not constant with temperature [39]. In spite of these limitations, a peak difference (ΔT_A) of 12.3 K is predicted at 10 kHz, which is comparable to 15 K observed for the difference in T_m between bulk and thin film form [21].

Eqs. (12) and (13) suggest that the permittivity measured with temperature is suppressed by the presence of strain in the film caused by the substrate. The significant conclusion from these two equations is that the strain largely contributes to the decrease in permittivity and greater dispersion observed in relaxor thin films compared to bulk. It has

been widely accepted that an order difference in the permittivity values observed between bulk and thin film ferroelectrics is due to the high strain levels, but the effect has not been quantified in this work for relaxors. Eq. (13) also reveals that the shape function ($\epsilon_A \delta_A^2$) will remain the same for both bulk and thin films. Since ϵ_A and δ_A^2 are inversely related, it can be concluded that if the permittivity is lower for the same material composition (thin film vs. bulk), it is always accompanied by a flatter dispersion response, which again is observed for our thin films in Fig. 3a.

By combining the dead layer and strain effect, the temperature dependence of thin film permittivity in the diffuse phase transition region can be related to the bulk by the following equation:

$$\begin{aligned} \frac{1}{\epsilon_{eff}} &= \frac{1}{(\epsilon_A)_{bulk}} - 4\epsilon_0 Q_{12} \\ &\times \frac{E_f}{1 - \nu_f} \left\{ x_{intrinsic} + \Delta\alpha \left[T_d - (T_A)_{bulk} + \frac{\Delta T_A}{2} \right] \right\} \\ &+ \frac{(t_{dead}/\epsilon_{dead})}{t} + \frac{[T - (T_A)_{bulk} + \Delta T_A]^2}{2(\epsilon_A)_{bulk}(\delta_A)_{bulk}^2} \end{aligned} \quad (14)$$

The thin film temperature-dependent permittivity for different thicknesses is predicted using Eq. (14) from the data reported in Ref. [21] for bulk PLZT (8/53/47) and compared to the experimental data, as shown in Fig. 7. A good agreement is observed between the predicted and measured DPT behavior of PLZT thin film, as illustrated in Fig. 7. The inset of Fig. 7 shows the shape parameter (δ_A) as a function of film thickness obtained for both the predicted and measured data in Fig. 7. It can be concluded that this modified Curie–Weiss law in Eq. (14) can be used to model the diffused phase transition in relaxor-based thin films on various substrates by utilizing known bulk material properties.

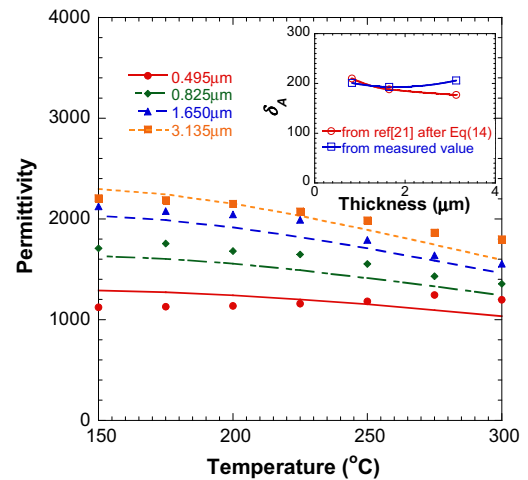


Fig. 7. Figure illustrates the calculated thin film permittivity (lines) for different PLZT thickness using bulk PLZT Ref. [21] and substrate material data using Eq. (14) and measured values (legends) from Fig. 3a for temperatures above T_m . Inset shows the comparison of shape parameter δ_A from the fitting and measured data.

4. Conclusion

The effect of dead layer and strain on the dielectric and DPT behavior of relaxor thin film was studied. It was found that the effect of dead layer on thin film permittivity is independent of frequency and temperature, and is governed by the Schottky barrier between platinum metal electrode and PLZT dielectric. The dead layer thickness between a platinum and PLZT dielectric was found to be 0.42 nm. The dead layer contributes only to the change in the permittivity and does not affect the maximum permittivity temperature (T_m). On the other hand, the total strain (thermal and intrinsic) contributes to both the extent of broadening and the shift in T_m . We modified the Curie–Weiss type law to include both these contributions to accurately predict the DPT behavior in thin film relaxors. The predicted behavior from bulk properties agreed well with the experimentally measured values in thin films. Such a model can be useful in selecting the substrate and electrode materials for developing relaxor thin films for different applications from bulk material properties.

Acknowledgements

This research was funded by the US Department of Energy, Office of Vehicle Technologies Program, under Contract No. DEAC02-06CH11357. The electron microscopy was carried out at the Electron Microscopy Center for Materials Research at Argonne National Laboratory.

References

- [1] Haertling GH. J Am Ceram Soc 1971;54:303.
- [2] Haertling GH, Land CE. J Am Ceram Soc 1971;54:1.
- [3] Haertling GH. J Am Ceram Soc 1999;82:797.
- [4] Cross LE. Relaxor ferroelectrics. In: Walter H, Karl L, Wolfram W, editors. Piezoelectricity. Berlin: Springer Verlag; 2008.
- [5] Cohen RE. Nature 2006;441:941.
- [6] Ye Z. Key Eng Mater 1998;155–156:81.
- [7] Viehland D, Li JF, Jang SJ, Cross LE, Wutting M. Phys Rev B: Condens Matter 1992;46:8013.
- [8] Pirc R, Blinc R. Phys Rev B: Condens Matter 2007;76:020101.
- [9] Bokov AA, Ye Z. J Mater Sci 2006;41:31.
- [10] Tyunina M. J Phys: Condens Matter 2006;18:5725.
- [11] Gregg JM. Phys Status Solidi A 2009;206:577.
- [12] Dawber M, Rabe KM, Scott JF. Rev Mod Phys 2005;77:1083.
- [13] Shaw TM, Trolier-McKinstry S, McIntyre PC. Annu Rev Mater Sci 2000;30:263.
- [14] Janolin PE. J Mater Sci 2009;44:5025.
- [15] Chang L, Alexe M, Scott JF, Gregg JM. Adv Mater 2009;21:4911.
- [16] Schwartz RW. Chem Mater 1997;9:2325.
- [17] Boyle TJ, Dimos D, Schwartz RW, Alam TM, Sinclair B, Buchheit CD. J Mater Res 1997;12:1022.
- [18] Lefevre MJ, Speck JS, Schwartz RW, Dimos D, Lockwood SJ. J Mater Res 1996;11:2076.
- [19] Sigman J, Brennecke GL, Clem PG, Tuttle BA. J Am Ceram Soc 2008;91:1851.
- [20] Sinnamon LJ, Saad MM, Bowman RM, Gregg JM. Appl Phys Lett 2002;81:703.
- [21] Gupta SM, J- Li, Viehland D. J Am Ceram Soc 1998;81:557.
- [22] Narayanan M, Ma B, Balachandran U, Li W. J Appl Phys 2010;107:024103.
- [23] Koch R. J Phys: Condens Matter 1994;6:9519.
- [24] Shaw TM, Suo Z, Huang M, Liniger E, Laibowitz RB, Baniecki JD. Appl Phys Lett 1999;75:2129.
- [25] Streiffer SK, Basceri C, Parker CB, Lash SE, Kingon AI. J Appl Phys 1999;86:4565.
- [26] H- Li, Si W, West AD, Xi XX. Appl Phys Lett 1998;73:464.
- [27] Taylor TR, Hansen PJ, Acikel B, Pervez N, York RA, Streiffer SK, et al. Appl Phys Lett 2002;80:1978.
- [28] Setter N, Damjanovic D, Eng L, Fox G, Gevorgian S, Hong S, et al. J Appl Phys 2006;100:051606.
- [29] Stengel M, Spaldin NA. Nature 2006;443:679.
- [30] Davis M, Damjanovic D, Setter N. Phys Rev B: Condens Matter 2006;73:014115.
- [31] Black CT, Welser JJ. IEEE T Electron Dev 1999;46:776.
- [32] Zafar S, Jones RE, Jiang B, White B, Kaushik V, Gillespie S. Appl Phys Lett 1998;73:3533.
- [33] Hwang CS. J Appl Phys 2002;92:432.
- [34] Sinnamon LJ, Bowman RM, Gregg JM. Appl Phys Lett 2001;78:1724.
- [35] Hwang CS, Lee BT, Kang CS, Lee KH, Cho H, Hideki H, et al. J Appl Phys 1999;85:287.
- [36] Majdoub MS, Maranganti R, Sharma P. Phys Rev B 2009;79:115412.
- [37] Ong RJ, Payne DA, Sottos NR. J Am Ceram Soc 2005;88:2839.
- [38] Bokov AA, Bing Y, Ye Z. Phys Rev B: Condens Matter 2003;68:052102.
- [39] Capanu M, Cervin-Lawry A, Patel A, Koutsaroff I, Woo P, Wu L, et al. Mater Res Soc Sympos Proc 2004;795:U11.29.1.